Order−Disorder Transition and Critical Micelle Temperature in Concentrated Block Copolymer Solutions

Moon Jeong Park and Kookheon Char*

School of Chemical Engineering & NANO Systems Institute, National Core Research Center (NCRC), Seoul National University, Seoul 151-744, Korea

Joona Bang and Timothy P. Lodge*

Department of Chemical Engineering & Materials Science, Department of Chemistry, University of Minnesota, Minneapolis, Minnesota 55455

Received November 9, 2004; Revised Manuscript Received December 30, 2004

ABSTRACT: The phase behavior of symmetric styrene−isoprene (SI) diblock copolymers in selective solvents in the vicinity of the order−disorder transition (ODT) was investigated by small-angle neutron scattering (SANS). Particular emphasis is placed on the region just above the ODT, where a disordered phase of micelles is observed. To understand morphological changes in more detail, one of the blocks is deuterated, i.e., PS−*d*PI and *d*PS−PI, and the scattering length density (SLD) of the solvents used were identical to the SLD of the corona chains. Two approaches for the analysis of SANS data were taken: the generalized indirect Fourier transformation (GIFT) and direct model fitting with relevant form and structure factors. With increasing temperature, the micellar aggregation number decreases, and the core radius is roughly maintained by the increased solvent swelling of the core. The critical micelle temperature (cmt) is experimentally described in the present study by an abrupt decrease in the size, aggregation number, and volume fraction of micelles. The micelles were found to dissociate into free chains approximately 20−30 °C higher than the T_{ODT}, and the cmt is found to be quite close to the mean-field spinodal temperature T_S. A mean-field temperature, T_{MF}, is located by the crossover temperature from the linear behavior of I_{max}^{-1} vs T^{-1} plot, and the structure factor above the experimentally determined T_{MF} is also found to be in good agreement with the Leibler−Landau-type mean-field theory. We examined two different ODTs: body-centered cubic lattices to disorder and hexagonal cylinders to disorder, with similar results in both cases.

Introduction

Numerous studies have been devoted to the fascinating phase transitions exhibited in block copolymers.[1−10] It is now well established both theoretically and experimentally for bulk diblock copolymers how the phase transitions (i.e., order−order and order−disorder transitions) depend on block composition and temperature. In particular, although the mean-field theory of Leibler[1] anticipates a first-order phase transition between a disordered melt and a bcc lattice of spherical micelles for any composition except for perfect symmetry, experimentally one finds the order−disorder transition to connect the disordered state directly to lamellae, hexagonal cylinders, double gyroid, or bcc spheres, depending on composition. Fredrickson and Helfand[3] argued that block copolymers fall in the Brazovskii universality class and that substantial spatial fluctuations in composition could stabilize the disordered phase, thereby accounting for the direct access to the various ordered states. Extensive experimental evidence of such fluctuations has been documented, and a variety of other theoretical approaches have also been brought to bear.[8−22] However, it is fair to say that a complete picture of the disordered state in the proximity of the ODT is still lacking.

One particularly interesting aspect of this regime arises for asymmetric copolymers, which adopt the bcc phase below the ODT.[9,10,23−30] Several authors observed that the disordered phase just above the ODT exhibited evidence of spherical micelles in a liquidlike state. The resulting ODT therefore reflects the loss of long-range order and identifiable symmetry, but does not result in complete homogenization of the blocks. Some authors have suggested distinguishing this ODT from that observed for gyroid, cylinder, or lamellar samples, by terming it the lattice disordering transition.[27−30] If there are distinct micelles present above the ODT, then at sufficiently high-temperature such micelles should disperse in favor of free chains. Evidence for a "critical micelle temperature" (cmt) has been presented in bulk diblocks, although it should be recognized that such a cmt does not represent a true thermodynamic phase transition.[26,30−33] It is of interest, therefore, to see whether such a "disordered micelle state" and an associated cmt can be observed in block copolymer solutions above the ODT.

Recently, Semenov's strong-segregation theory[34] for highly asymmetric block copolymers was extended to consider the possible stability of a disordered micelle regime above the ODT.[26] The existence of disordered micelles was indeed confirmed in sphere-forming diblock copolymers at elevated temperatures,[28−30] in contrast to classical mean-field calculations.[1,35,36] Experimentally,[31] detailed analysis of SANS data in the bulk suggests that the micelles remain relatively unchanged as the temperature is increased, but their number density and volume fraction decrease steadily.

Although considerable attention has already been paid to micellization in dilute solutions, there have been fewer reports on concentrated block copolymer solutions.

* Authors for correspondence: (K.C.) khchar@plaza.snu.ac.kr; (T.P.L) lodge@chem.umn.edu.

10.1021/ma0477044 CCC: $30.25
Published on Web 02/16/2005

Pioneering studies on block copolymer solutions were performed by Hashimoto and co-workers.[37,38] For asymmetric polystyrene-polybutadiene (PS−PB) block copolymers in the PB-selective solvent tetradecane (C14), Hashimoto and co-workers found that at a fixed concentration, increasing temperature leads to a loss of long-range order, signaling a melting from an ordered lattice to a liquidlike micellar solution; at even higher temperatures, the micelles eventually dissolve into a homogeneous solution.

Hamley and co-workers[39] investigated the phase behavior of asymmetric PS−PI and PS−PI−PS block copolymers in the PS-selective solvent di-*n*-butylphthalate (DBP). The hexagonal cylinder (hex) and lamellar microstructures in the concentration range $0 \leq \phi \leq 0.4$ dissolve into micellar solutions at T_{ODT}. Above T_{ODT} there is a significant range of temperature over which the micellar interactions persist before the micelles are fully dissociated. On the basis of a combination of SAXS and rheology measurements, they proposed an "approximate phase diagram" where the micelles were dissociated into free chains approximately 30 °C above the T_{ODT}. The ODT temperature in concentrated block copolymer solutions was found to be essentially independent of concentration and it is also interesting to note that the ODTs in concentrated solutions coincided with the cmts in dilute solutions, indicating that the ODT is dictated by the PI-solvent interaction, rather than the PI−PS block interaction.[40,41]

The work by Hamley and co-workers[39] raises two fundamental issues: (1) What would the effect of the addition of a selective solvent on the ODT of *symmetric* diblock copolymers be? (2) Is there any difference in structure and other characteristics of disordered micelles caused by different ordered microstructures, i.e., body-centered cubic (bcc) and hex, prior to the disordered state?

In this study, we examine nondilute block copolymer solutions, focusing on a symmetric diblock copolymer in selective solvents. To investigate the structural features in the disordered micelle regime, a detailed experimental examination of two ODTs is presented: from bcc spheres and from hexagonal cylinders. To clarify two structural aspect of block copolymer solutions with SANS, one of the blocks is deuterated and solvents selective to the protonated block were used, i.e., PS-*b*-*d*PI in dialkyl phthalates and *d*PS-*b*-PI in tetradecane. The ODT is defined in the present study as the transition temperature from the bcc or hex phase to disordered micelles and the cmt as the temperature for the dissolution of micelles. A qualitative criterion for the cmt is also suggested by the SANS data. In a related study, the detailed micellar characteristics of the same copolymers were studied by SANS in dilute solution, as a function of temperature up to the cmt.[42]

Experimental Section

Materials. Two nearly symmetric diblock copolymers were synthesized by a standard anionic polymerization procedure.[40] One copolymer, designated S*d*I(15−14), incorporated protonated styrene and perdeuterated isoprene, while the other, designated *d*SI(16−15), had perdeuterated styrene and protonated isoprene. The deuterated monomers were purchased from Polymer Source, Inc. Styrene (protonated or perdeuterated) was purified by stirring over calcium hydride for 12 h, followed by vacuum distillation with *n*-butyllithium for 6 h. Isoprene (protonated or perdeuterated) was treated with dibutylmagnesium for 3 h, followed by *n*-butyllithium for 6 h.

Table 1. Scattering Length Densities (SLDs) of Materials Used in Present Study

species	formula	mol wt (g/mol)	density (g/cm^3)	scattering length density (10^{-6} Å^{-2})
PS	C_8H_8	104.15	1.047	1.41
*d*PS	C_8D_8	112.22	1.128	6.45
PI	C_5H_8	68.12	0.913	0.27
*d*PI	C_5D_8	76.09	0.986	6.75
DEP	$C_{12}H_{14}O_4$	232.16	1.118	1.53
DBP	$C_{16}H_{22}O_4$	278.35	1.043	1.07
C14	$C_{14}H_{30}$	198.40	0.763	−0.44
*d*C14	$C_{14}D_{30}$	228.66	0.882	6.81

Cyclohexane was used as the polymerization solvent and was distilled from *n*-butyllithium. Using *sec*-butyllithium as an initiator, the styrene was polymerized for 4 h at 45 °C, followed by the addition of isoprene and polymerization for 4 h at the same temperature.

The polymers were characterized by size exclusion chromatography (SEC) equipped with both refractive index and multiangle light scattering detectors (Wyatt Optilab and Dawn), and by ^{1}H NMR spectroscopy. A small amount of the styrene block was sampled before adding the isoprene monomer and SEC yielded number-average molecular weights of 14100 (PS) and 15400 (*d*PS) with polydispersity indices around 1.02. After growing the isoprene block, a light scattering instrument was incorporated in the SEC apparatus to determine the absolute molecular weight.[43] The refractive index increment was determined with a differential refractometer independently, and this value was then used in the analysis of the chromatogram.[44] The resulting block molecular weights were 15400 (S) and 14100 (*d*I) g/mol for S*d*I(15−14) and 15800 (*d*S) and 15400 (I) g/mol for *d*SI(16−15), respectively. The polydispersity indices for both S*d*I(15−14) and *d*SI(16−15) are 1.04. ^{1}H NMR spectroscopy (Varian VXR-500 MHz) was used to determine the composition and to estimate the mole percent of 1,4-addition of the PI block (94 ± 1%). Two PS-selective solvents, diethyl phthalate (DEP) and di-*n*-butyl phthalate (DBP), and one PI-selective solvent, *n*-tetradecane (C14), were obtained from Aldrich. Perdeuterated tetradecane (*d*-C14) was obtained from C/D/N Isotope Inc.

Solutions of S*d*I(15−14) in a mixture of 75:25 vol % DEP:DBP and *d*SI(16−15) in C14 were prepared with polymer concentrations of 25 and 40 vol % using CH_2Cl_2 as a cosolvent; the CH_2Cl_2 was later removed under a gentle flow of nitrogen until the solution reached a constant weight. The 25% and 40% solutions were intentionally chosen to access the bcc/disorder and hex/disorder transitions, respectively, as a function of temperature.[40,41,45]

Small-Angle Neutron Scattering (SANS). SANS measurements were performed using the 30 m NG7 beamline at the National Institute of Standards and Technology (NIST). A sample-to-detector distance of 7.05 m and a neutron wavelength (λ) of 6 Å with $\Delta\lambda/\lambda = 0.10$ were used to access scattering vectors q ($q = 4\pi\sin(\theta/2)/\lambda$, where θ is the scattering angle) in the range 0.064−0.975 nm^{-1}. A heated sample chamber was employed for temperature control, with an accuracy of ± 0.1 °C. The typical exposure time was 5 min at a given temperature and each solution was annealed for at least 10 min at a given temperature before measurement. For S*d*I(15−14), a mixture of PS-selective solvents DEP and DBP with a volume ratio of 3 to 1, was chosen for the contrast matching of the scattering length density (SLD) with the PS coronas in the micelles, thereby enabling detailed examination of the *d*PI cores. The contrast matching method was also applied to *d*SI(16−15) by using a mixture of tetradecane (C14) and deuterated tetradecane (*d*C14) with a volume ratio of 9 to 1. Since C14 is selective for the PI block, the *d*PS core dominates the SANS. The solutions were placed between two sealed quartz windows with a flight path of ca. 1 mm. SLDs and molecular characteristics of materials used for the SANS experiments are summarized in Table 1.

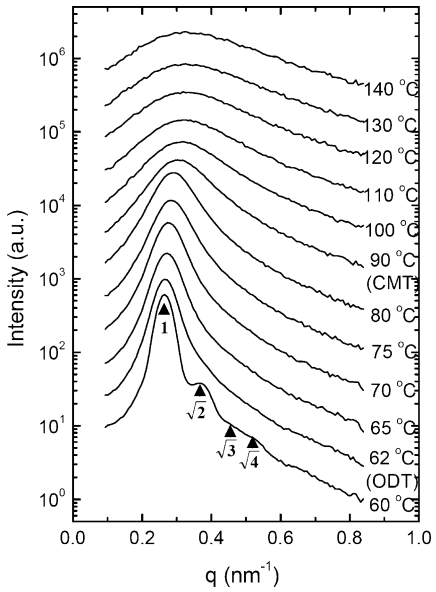

Figure 1. SANS profiles for a 25% SdI(15−14) in DEP/DBP (75/25 vol %) solution as a function of temperature. The filled triangles for the SANS profile at 60 °C indicate the Bragg reflections corresponding to the bcc phase. Each profile is shifted vertically by half a decade relative to the profile for immediately previous temperature for clarity. T_{ODT} is located at 62 °C and we also observed an abrupt decrease in the peak intensity at around 90 °C, which is attributed to the cmt.

Results and Discussion

ODT from Bcc Microstructure. Figure 1 presents the SANS profiles (scattering intensity $I(q)$ against scattering vector **q**) for the 25% S*d*I(15−14) in DEP/DBP measured at different temperatures to show the behavior at and above the ODT in more detail. Each scattering profile was shifted vertically for clarity. The scattering intensity decreases significantly with increasing temperature indicating the classical UCODT-type phase behavior. Below 60 °C, the higher order peaks at $\sqrt{2}q_{max}$, $\sqrt{3}q_{max}$, and $\sqrt{4}q_{max}$ indicate the microphase-separated bcc structure, which completely disappear at a temperature between 60 and 62 °C. Consequently, the T_{ODT} is considered to be located between 60 and 62 °C. Around 90 °C, there is an additional abrupt decrease in the peak intensity and increase in peak width, which we attribute to the cmt at which the micelle-to-free chain equilibrium is shifted toward the free chains. Upon further heating, the main peak intensity originating from the intermicellar interaction becomes negligible, with only the broad correlation hole contribution remaining, indicating a fully disordered copolymer solution.

To facilitate the comparison of experimental data obtained here with theory, the inverse peak intensity, I_{max}^{-1}, the square of the full-width at half-maximum (fwhm) of the main peak, σ_q^2, and the characteristic length D defined by $D = 2\pi/q_{max}$ with q_{max} being the scattering vector at the first peak position, are plotted against the inverse of absolute temperature, T^{-1}, as shown in Figure 2. The first-order transition at T_{ODT} = 62 °C is confirmed in the insets via discontinuous changes in both I_{max}^{-1} and σ_q^2. In the disordered state of block copolymers, the mean-field theory[1] for a UCODT-type block copolymer predicts that both I_{max}^{-1} and σ_q^2 are proportional to T^{-1}. As shown in Figure 2, both I_{max}^{-1} and σ_q^2 exhibit a fairly wide region of linear

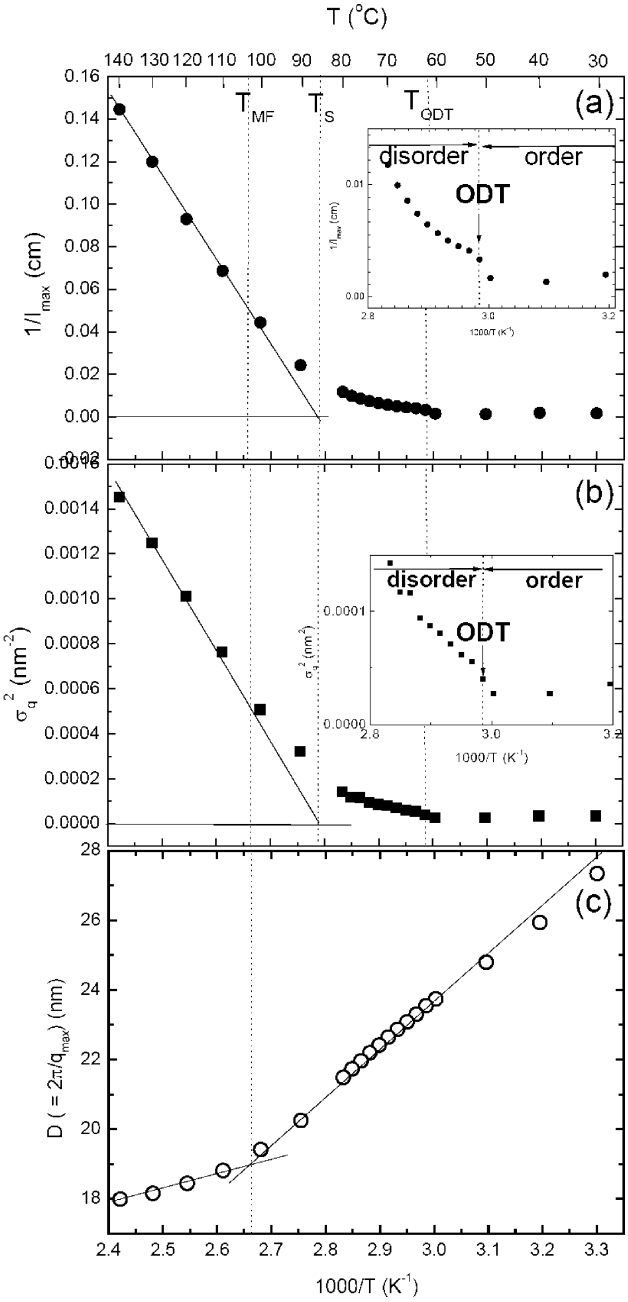

Figure 2. Temperature dependence of (a) I_{max}^{-1}, (b) σ_q^2, and (c) D for a 25% S*d*I(15−14) in DEP/DBP (75/25 vol %) solution. The lines in parts a and b are fitted to the data as predicted from the mean-field theory. Insets in parts a and b highlight the discontinuous change in both quantities near the ODT. The positions of mean-field temperature (T_{MF}), spinodal temperature (T_S), and order−disorder transition temperature (T_{ODT}) are also indicated in the figure.

behavior with respect to T^{-1}. The thermal fluctuation effect near the ODT is known to cause a deviation from the linear relationship and the crossover temperature from the mean-field to the thermal fluctuation regime in the disordered state was defined as T_{MF}. We also note in Figure 2 that there is a clear-cut crossover of D upon heating the sample through the mean-field temperature, and T_{MF} = 104 °C was thus determined. The mean-field spinodal temperature, T_S = 86 °C, is defined by the temperature at which both I_{max}^{-1} and σ_q^2 become zero by the linear extrapolation from the mean-field region. It is intriguing to note that the mean-field spinodal

temperature T_S is quite close to the cmt as defined in Figure 1.

We have taken two approaches for the analysis of the SANS data to investigate the disordered micelle regime in more detail. One employs the model-independent generalized indirect Fourier transformation (GIFT) developed by Glatter and co-workers[46] and the other uses direct model fitting with relevant form and structure factors. The GIFT method separates the form factor $P(q)$ (i.e., intraparticle scattering) and the structure factor $S(q)$ (i.e., interparticle scattering) contributions. In the case of a uniform dispersion of monodisperse, homogeneous, and isotropic spherical particles, no orientation effect is taken into account so that the total scattering intensity $I(q)$ can be written

$$I(q) = NP(q)\mathrm{S}(q) \tag{1}$$

where N is the number of particles. From the form factor $P(q)$, it is possible to obtain the pair distance distribution function, $p(r)$, by the spatially averaged Fourier transformation:

$$P(q) = 4\pi\int_0^\infty p(r)\frac{\sin(qr)}{qr}\,\mathrm{d}r \tag{2}$$

In real (r) space, the interparticle interactions are described by the total correlation function $h(r) = g(r) - 1$ with $g(r)$ being the radial distribution function and r the distance between the centers of two particles.[47] Using the relationship between functions in q and r space, $S(q)$ and $h(r)$, similar to the pair of $P(q)$ and $p(r)$, form another Fourier transform pair:

$$S(q) = 1 + 4\pi n\int_0^\infty h(r)r^2\frac{\sin(qr)}{qr}\,\mathrm{d}r \tag{3}$$

Equation 1 applies to the case of an isotropic dispersion of monodisperse spherical particles. However, it has been shown with many examples that by introducing the "averaged structure factor" $S^{ave}(q)$, with the average taken over the weighted contributions of partial structure factors for individual monodisperse systems. More exactly the "effective structure factor" $S^{eff}(q)$ can produce improved experimental data fit for polydisperse spheres or cylinders[48] and even for inhomogeneous particles.[46,49] In this case $S^{eff}(q)$ is no longer a single function of the particle distribution in space, but depends on the form amplitudes of the particles. As a result, the structure factor is replaced by the effective structure factor[49]

$$I(q) = N\overline{P(q)}S^{eff}(q) \tag{4}$$

where $\overline{P(q)}$ is the appropriately averaged form factor. The structure factor $S(q)$ is determined by means of a nonlinear least-squares method, and a Lagrange multiplier is systematically varied until the optimum solution is obtained. The $S(q)$ involves up to four adjustable parameters for a given interaction model. We find that the Percus−Yevick (PY) average hard-sphere model, combined with an unconstrained form factor for a polydisperse system, fits the data quite well at temperatures above the ODT.

Figure 3a shows typical pair distance distribution functions, $p(r)$, at different temperatures for the 25% solution and the decrease in the dPI core size with the increase in temperature is clearly visible. The resulting number-average micelle core radii, R_c, extracted from

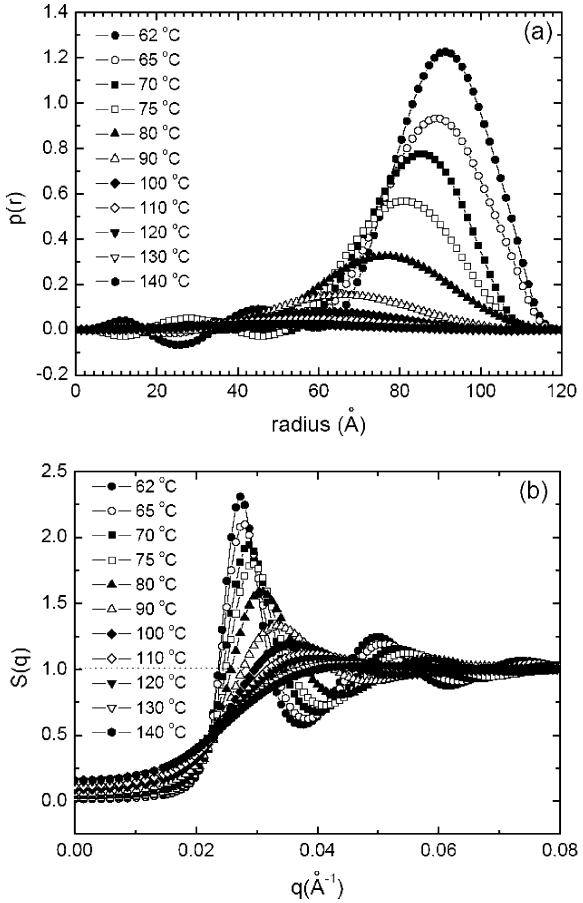

Figure 3. Representative (a) pair distance distribution functions, $p(r)$, and (b) structure factors, $S(q)$, obtained from the GIFT at indicated temperatures for a 25% SdI(15−14) in DEP/DBP (75/25 vol %).

Table 2. Summary of GIFT Fitting Parameters for a 25% SdI(15−14) in DEP/DBP (75/25 vol %)

T, °C	R_c, Å	R_{hs}, Å	$R_{hs} - R_c$, Å	N_{agg}	ϕ_{hs}
62	91.4	129.9	38.5	135	0.510
65	88.6	125.6	37.0	123	0.494
70	85.9	121.6	35.7	112	0.474
75	81.0	115.2	34.2	94	0.441
80	76.4	110.6	34.2	79	0.415
90	65.5	100.1	34.6	49	0.325
100	61.4	92.6	31.2	41	0.308
110	57.3	86.8	29.5	33	0.284
120	50.5	83.4	32.9	23	0.243
130	50.5	80.5	30	23	0.241
140	49.1	79.2	30.1	21	0.236

$p(r)$ are listed in Table 2. Since the shape of $p(r)$ is found to be sensitive to the upper bound on R_{max}, R_{max} was carefully varied to obtain the best fit. There are small oscillations for $R_c < 60$ Å, probably due to the noise in the data at high q and the instrumental smearing. The corresponding structure factors for the 25% solution at different temperatures obtained from the GIFT analysis are also shown in Figure 3b. The parameters need to determine the structure factor are the effective hard sphere radius, R_{hs}, and the volume fraction of effective hard spheres, ϕ_{hs}. As summarized in Table 2, R_c and ϕ_{hs} decrease steadily for the entire temperature region covered, while the difference between R_{hs} and R_c related to the effective thickness of corona remains almost constant with a value between 3.0 and 3.9 nm. The aggregation number of the micelles, assuming no solvent in core, can be estimated from the core size and

the molecular volume of the *d*PI block based on the relationship

$$N_{agg} = \frac{4\pi {R_c}^3}{3V_{dPI}} = \frac{4\pi {R_c}^3}{3}\frac{\rho_{dPI} N_A}{M_{dPI}} \quad (5)$$

where N_A is Avogadro's number, ρ_{dPI} is the density of the *d*PI block, and M_{dPI} is the molecular weight of the *d*PI block. At 62 °C, the calculated N_{agg} is 135, and this value is in fair agreement with the N_{agg} estimated directly from the q_{max} value as follows. At 60 °C, when the solution forms the bcc lattice

$$N_{agg} = \frac{volume\ per\ one\ micelle}{volume\ per\ one\ chain} = \frac{\phi(a^3/2)f_{core}}{molecular\ volume\ of\ core/N_A} \quad (6)$$

where a is the lattice parameter, $a = \sqrt{2}d_{110} = \sqrt{2}(2\pi/q_{max})$, ϕ is the polymer volume fraction, and f_{core} is a volume fraction of the core block. The N_{agg} calculated from eq 6 is 152. This value lies slightly above the value obtained by the fitting with SANS data since the calculation by eq 6 assumes that all chains are in micelles. It is interesting to note that we observed a significant decrease in ϕ_{hs} at around 90 °C, which is believed to be the cmt, as mentioned in Figures 1 and 2. Additionally, the oscillations in $S(q)$, indicative of correlations among micelles, almost disappear. This observation implies that the block copolymer chains incorporated into the micelles are dissociated to free chains around this temperature (i.e., cmt). The validity of the model fit using eq 4 to scattering profiles above the cmt will be discussed in later.

To confirm the micellar size and the shape, different models of the form factor have been tested to fit the SANS data. A micellar form factor shown in eq 7 consists of the self-correlation of a core, the self-correlation of a corona, the cross-terms between the core and the corona, as well as between different corona chains:[50,51]

$$P_{micelle}(q) = N\Delta\rho_{core}{}^2 P_{core}(q) + N\Delta\rho_{corona}{}^2 P_{corona}(q) + 2N\Delta\rho_{core}\Delta\rho_{corona}S_{core-corona}(q) + N(N-1)\Delta\rho_{corona}{}^2 S_{corona-corona}(q) \quad (7)$$

where $\Delta\rho$ is the contrast of scattering length density (SLD) between core (or corona) and solvent. This expression was also used in our study of the same copolymers in dilute solution.[42] Since we took advantage of the contrast matching in SLD between the solvent and the corona (i.e., $\Delta\rho_{corona} = 0$), the micelle form factor shown in eq 7 can be significantly simplified to

$$P_{micelle}(q) = N\Delta\rho_{core}{}^2 P_{core}(q) \quad (8)$$

If we assume a sphere form factor for a spherical micelle with uniform SLD, the micelle form factor can be written as

$$P_{micelle}(q,R_c) = \left[\left(\frac{4\pi}{3}{R_c}^3\right)\Delta\rho_{core}\frac{3J_1(qR_c)}{qR_c}\right]^2 \quad (9)$$

where $J_1(x)$ ($J_1(x) = (\sin(x) - x\cos(x))/x^2$) is the first-order spherical Bessel function. The polydispersity in R_c is taken into account by convoluting the spherical form factor with the Gaussian distribution. Consequently, the $P(q)$ becomes

$$P(q, R_c, \sigma_c) = \int_0^\infty \exp\left(\frac{-(R-R_c)^2}{2{\sigma_c}^2}\right) P_{micelle}(q, R_c)\, dR \quad (10)$$

where σ_c is the width of the distribution.

We also need to take into account the Percus−Yevick (PY) structure factor, $S(q)$, as shown in eq 11 below in order to fit the SANS data, to describe the intermicellar interaction based on hard spheres

$$S(q) = \frac{1}{1 + 24\phi_{hs}G(2qR_{hs})/(2qR_{hs})} \quad (11)$$

where G is a trigonometric function of $A = 2qR_{hs}$ and ϕ_{hs} given below:

$$G(A) = \left(\frac{(1+2\phi_{hs})^2}{(1-\phi_{hs})^4}\right)\left(\frac{\sin A - A\cos A}{A^2}\right) - \left(\frac{6\phi_{hs}(1+0.5\phi_{hs})^2}{(1-\phi_{hs})^4}\right)\left(\frac{2A\sin A + (2-A^2)\cos A - 2}{A^3}\right) + \left(\frac{0.5\phi_{hs}(1+2\phi_{hs})^2}{(1-\phi_{hs})^4}\right) \times ([-A^4\cos A + 4\{(3A^2-6)\cos A + (A^3-6A)\sin A + 6\}]/A^5) \quad (12)$$

In the end there are four independent parameters involved in fitting the model-specific scattering intensity: a micelle core radius, R_c, a polydispersity in micellar core radius, σ_c, an effective hard-sphere radius, R_{hs}, and a volume fraction of effective hard spheres, ϕ_{hs}.

The calculated neutron scattering intensity is also smeared to fit the measured SANS intensity $I(q_0)$ considering the instrumental resolution function, which can be approximated by the Gaussian function as follows:[52]

$$I(q_0) = \int I(q)\frac{1}{\sqrt{2\pi}\sigma_q}\exp\left(-\frac{1}{2}\left(\frac{q-q_0}{\sigma_q}\right)^2\right) dq \quad (13)$$

where σ_q is determined by the monochromaticity of neutron wavelength, detector resolution, and instrumental geometry. It is, however, noted that in these solutions σ_q plays a minor role in determining the scattering parameters.

Figure 4 shows the comparison of the SANS data at 70 °C with the model fits based on both the GIFT and the PY model with a spherical form factor. Both models are in excellent agreement with our experimental data. The resulting parameters obtained from the specific model fits are summarized in Table 3. Note that the R_c, R_{hs}, and ϕ_{hs} values are in close agreement with the values obtained from the GIFT analysis. However, it is quite feasible that a significant amount of solvent can exist within the micelle core near the ODT. If the solvent

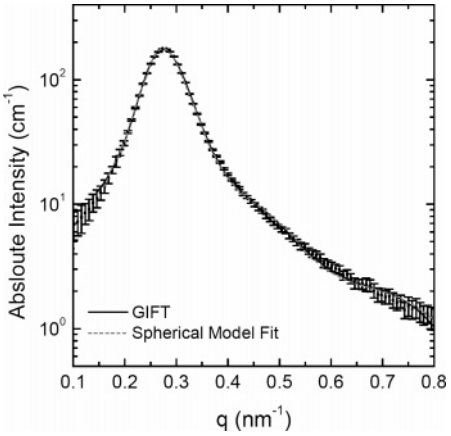

Figure 4. SANS scattering profile for a 25% S*d*I(15−14) in DEP/DBP (75/25 vol %) solution at 62 °C fitted with both the GIFT and the PY effective hard-sphere model with a spherical form factor.

Table 3. Summary of Parameters Obtained from the Percus−Yevick Hard Sphere Model Fits for a 25% S*d*I(15−14) in DEP/DBP (75/25 vol %)

T, °C	R_c, Å	R_{hs}, Å	$R_{hs} - R_c$, Å	N_{agg}	$\phi_{core,\,sol}$	σ_c	ϕ_{hs}
62	87.1	130.0	42.9	70	0.395	6.3	0.510
65	85.2	125.5	40.3	63	0.422	7.3	0.498
70	82.3	122.0	39.7	55	0.444	7.3	0.470
75	79.0	115.5	36.5	44	0.491	7.7	0.445
80	73.6	110.0	36.4	35	0.504	8.2	0.415
90	60.8	98.3	37.5	19	0.527	8.0	0.325
100	58.4	92.6	34.2	14	0.613	11.1	0.310
110	56.1	86.5	30.4	11	0.659	12.3	0.285
120	50.5	83.1	32.6	8	0.668	11.1	0.250
130	49.6	79.2	29.6	7	0.686	12.4	0.245
140	49.1	78.5	29.4	6	0.706	14.2	0.238

is allowed to exist within the micelle core (*d*PI in present study), the $\Delta\rho$ in eq 9 is rewritten below:

$$\Delta\rho = \left[\frac{3N_{agg}V_{dPI}}{4\pi R_c^{\,3}}\rho_{dPI} + \left(1 - \frac{3N_{agg}V_{dPI}}{4\pi R_c^{\,3}}\right)\rho_S\right] -$$

$$\rho_S = \frac{3N_{agg}V_{dPI}}{4\pi R_c^{\,3}}(\rho_{dPI} - \rho_S) \quad (14)$$

The resulting aggregation numbers and volume fractions of solvent in the micelle core are also listed in Table 3. It is interesting to note that the decrease in aggregation number is offset by the increased solvent swelling of the micelle core as the temperature is increased. Above the cmt, the obtained aggregation number is found to be below 20 and the volume fraction of solvent in the micelle core is above 50%, implying that micelles start to break up into free chains at approximately 30 °C higher than T_{ODT}. Upon further heating, the aggregation number decreases below 10 and the solvent is estimated to exist in the micelle core as much as 70%. It is, however, noted here that the SANS profiles in disordered state, particularly above T_{MF} should be analyzed by the Leibler's mean-field theory in order to obtain more reasonable results. Therefore, the model fit using eqs 8 to 14 qualitatively indicates that there is a significant decrease in micelle number density above the cmt.

Effect of Solvent Selectivity. The universality of these phenomena can be explored by inverting the solvent selectivity, i.e., to place the PS blocks in the micellar cores. SANS measurements for a 25% solution

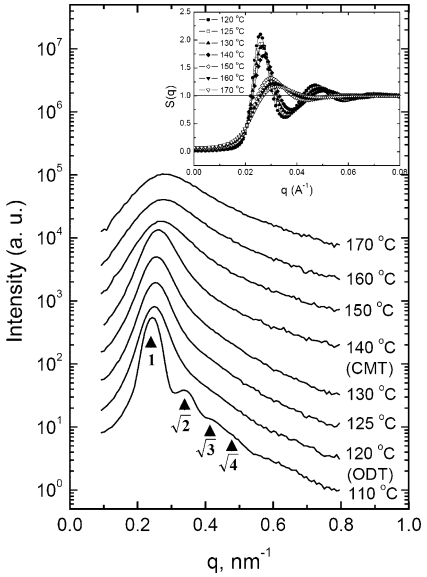

Figure 5. SANS profiles for a 25% *d*SI(16−15) in C14/*d*C14 (90/10 vol %) with the increase in temperature. The filled triangles for the SANS profile at 115 °C indicate the Bragg reflections corresponding to bcc phase. Each profile is shifted vertically by half a decade relative to the profile for immediately previous temperature for clarity. T_{ODT} is located at 120 °C and an abrupt decrease in the peak intensity, which is related to the cmt, was observed at around 140 °C. The structure factors obtained from the GIFT model are also shown in the inset.

Table 4. Summary of GIFT Fitting Parameters for a 25% *d*SI(16−15) in C14/*d*C14 (90/10 vol %)

T, °C	R_c, Å	R_{hs}, Å	$R_{hs} - R_c$, Å	ϕ_{hs}
120	97.5	138.7	41.2	0.515
122	96.2	137.1	40.9	0.508
124	95.0	135.8	40.8	0.502
126	94.0	134.7	40.7	0.497
128	92.7	133.1	40.4	0.490
130	91.3	131.7	40.4	0.483
135	90.0	130.9	40.9	0.476
140	89.3	128.8	39.5	0.466
150	78.8	115.2	36.4	0.396
160	73.3	109.4	36.1	0.355
170	69.1	105.2	36.1	0.334

of *d*SI(16−15) in C14/*d*C14 (90/10 vol %) solution were carried out, which also undergoes the bcc-to-disordered transition. As shown in Figure 5, the solution shows the ODT between 110 and 120 °C and a distinct cmt between 130 and 140 °C. The data were analyzed by GIFT in exactly the same manner as for S*d*I(15−14) in DEP/DBP. As shown in the inset of Figure 5, the first peak intensities of the structure factors at different temperatures above the ODT decrease considerably when undergoing the cmt, and the oscillation of the structure factor eventually disappears upon further heating. The decrease in the *d*PS core size with the increase in temperature is again clearly represented as summarized in Table 4. In particular, we observed an abrupt decrease in R_c around the cmt, which is similar to the behavior obtained with the 25% S*d*I(15−14) in DEP/DBP. As shown in Table 4, the ϕ_{hs} gradually decreases throughout the temperature range covered in present study, and most notably, a significant decrease in ϕ_{hs} near the cmt is again detected. Similar features of I_{max}^{-1}, σ_q^2, and $p(r)$ against temperature were obtained with the 25% *d*SI(15−14) in C14/*d*C14, as shown in Figure 6. The experimentally determined T_{ODT}, T_S, and T_{MF} are about 121 °C, 140 °C, and 152 °C,

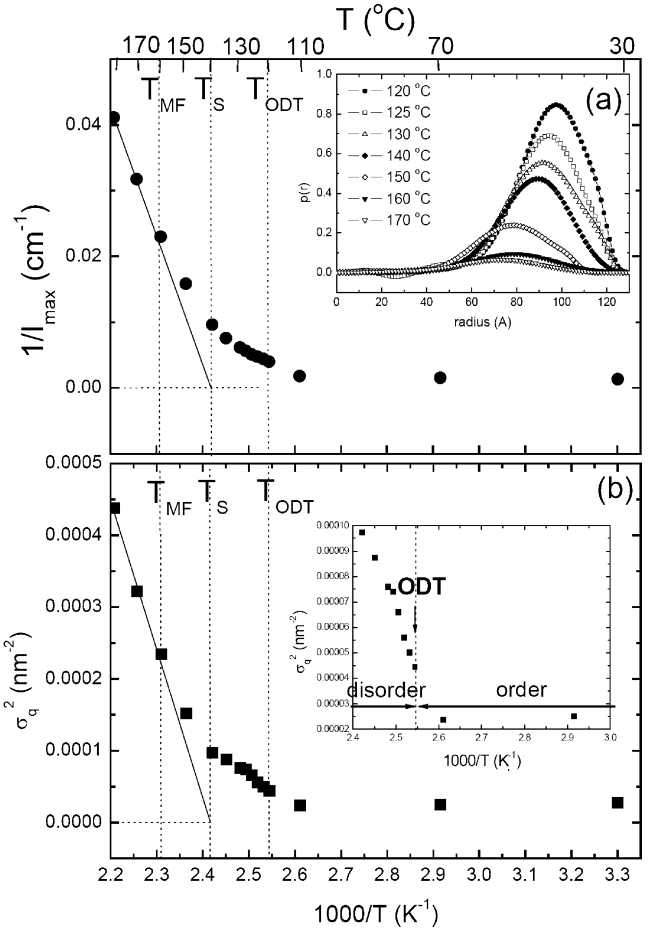

Figure 6. Temperature dependence of (a) I_{max}^{-1} and (b) σ_q^2 for a 25% *d*SI(16−15) in C14/*d*C14 (90/10 vol %) solution. The lines in parts a and b are fitted to the data as predicted from the mean-field theory. The inset in part a shows the pair distance distribution functions, $p(r)$, and the inset in part b highlights the discontinuous change near the ODT. The mean-field temperature (T_{MF}), spinodal temperature (T_S), and order−disorder transition temperature (T_{ODT}) are also located in the figure.

respectively. It is again interesting to note that the mean-field spinodal temperature T_S is close to the cmt as discussed in Figures 1 and 2. It is also worthwhile to note at this point that the temperature difference between the ODT and the cmt is about 20−30 °C for both solutions undergoing the bcc-to-disorder transition, independent of solvent. Detailed analysis of the SANS profiles in the disordered state above T_{MF} will be given later via mean-field theory.

ODT from Hex Lattices. SANS experiments were also performed for a 40% S*d*I(15−14) in DEP/DBP undergoing the hex-to-disorder transition. Figure 7 shows the corresponding SANS profiles (shifted vertically for clarity) upon heating. The typical UCODT-type phase behavior was observed. Below 78 °C, the higher order peaks at $\sqrt{3}q_{max}$ and $\sqrt{4}q_{max}$ peaks clearly indicate the hex microstructure, which disappear at a temperature between 78 and 80 °C. As a result, the T_{ODT} is located between 78 and 80 °C. Using the same criterion for the cmt established in Figure 1, we observe the onset of cmt at around 100 °C. However, the extent of the decrease in the peak intensity near the cmt is not as distinct for the higher concentration. Upon further heating, the broad scattering maximum is consistent with a fully disordered block copolymer solution.

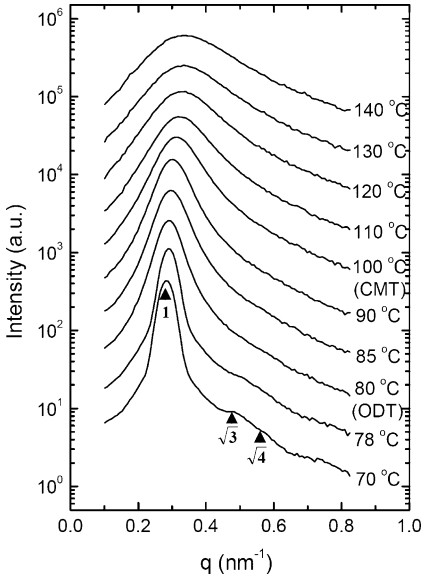

Figure 7. SANS profiles for a 40% S*d*I(15−14) in DEP/DBP (75/25 vol %) solution as a function of temperature. The filled triangles for the SANS profile at 70 °C indicate the Bragg reflections corresponding to the hexagonal cylinder phase. Each trace is shifted vertically by half a decade relative to the profile for immediately previous temperature for clarity. Both T_{ODT} and cmt are located at 80 and 100 °C, respectively, in the figure.

Different behavior of the disordered micelles by changing the polymer concentration can be shown by the plots of I_{max}^{-1}, σ_q^2, and D against T^{-1}, as presented in Figure 8. The distinct T_{ODT} = 80 °C is located by the discontinuities in both I_{max}^{-1} and σ_q^2. From the T^{-1} dependence of D, $T_{MF} \approx 120$ °C was determined. In the same way as shown in Figure 2, the mean-field spinodal temperature, $T_S \approx 100$ °C, which is related to the cmt as denoted in Figure 7, is determined. However, that the change of the slope of D plotted against T^{-1} near T_{MF} for the 40% solution is quite small compared with the visible change for the 25% solution. In fact, above the hex-to-disorder transition the cmt is harder to find compared with the bcc-to-disorder transition. We speculate that the difference arises because the cmt in the hex case is for a higher concentration solution, and the fully disordered fluid scattering (the "correlation hole" peak) is proportionally stronger; consequently, there is simply less difference between the disordered liquid and disordered micelle scattering. This interpretation is supported by previous work in melts, where the cmt was very hard to locate precisely.[31]

The GIFT analysis was also applied to obtain information on the micelle size and hard sphere volume fraction. The results are given in Table 5. Similarly, the PY average hard-sphere model, combined with an unconstrained form factor for a polydisperse system, also fits the data quite well and the fitting results are summarized in Table 6. The main features of the parameters obtained from the model fit are qualitatively similar to the case with bcc-to-disorder transition (i.e., 25% solutions). Figures 9a and 9b show the pair distance distribution functions, $p(r)$, and the structure factors $S(q)$ at different temperatures, respectively. The decrease in the *d*PI core size with almost constant effective corona thickness (ca. 3.1−3.7 nm) and the steady decrease in ϕ_{hs} upon heating are again observed. A notable decrease in R_c around 100 °C, which is believed to be the cmt, is again present although it was

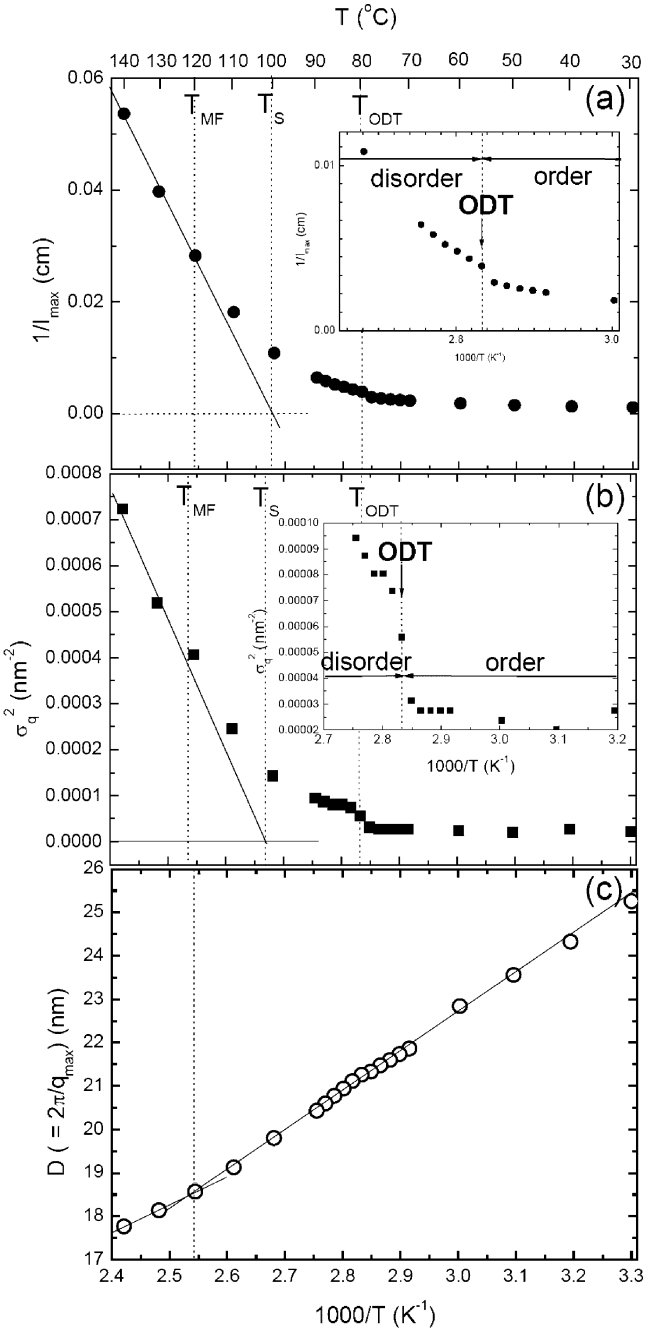

Figure 8. Temperature dependence of (a) I_{max}^{-1}, (b) σ_q^2, and (c) D for a 40% SdI(15−14) in DEP/DBP (75/25 vol %) solution. The lines in parts a and b are fitted to the data as predicted from the mean-field theory. Insets in parts a and b highlight the discontinuous change in both quantities near the ODT and the positions of T_{MF}, T_S, and T_{ODT} are indicated in the figure.

Table 5. Summary of GIFT Fitting Parameters for a 40% SdI(15−14) in DEP/DBP (75/25 vol %)

T, °C	R_c, Å	R_{hs}, Å	$R_{hs} - R_c$, Å	ϕ_{hs}
80	81.8	118.5	36.7	0.525
85	79.5	114.4	34.9	0.492
90	77.7	111.6	33.9	0.479
100	70.9	104.1	33.2	0.445
110	62.7	98.0	35.3	0.392
120	60.5	92.7	32.7	0.383
130	57.7	89.3	31.6	0.351
140	55.9	86.4	30.5	0.318

harder to locate the cmt from the scattering profiles given in Figure 7. However, it should be mentioned here that the extent of decrease in R_c and ϕ_{hs} for the hex-to-disorder transition is approximately half what it was for the bcc-to-disorder transition. Above the cmt, the oscillations in the correlation functions gradually disappear and eventually level off to unity, implying the low intermicellar correlation due to the formation of dominant free chains.

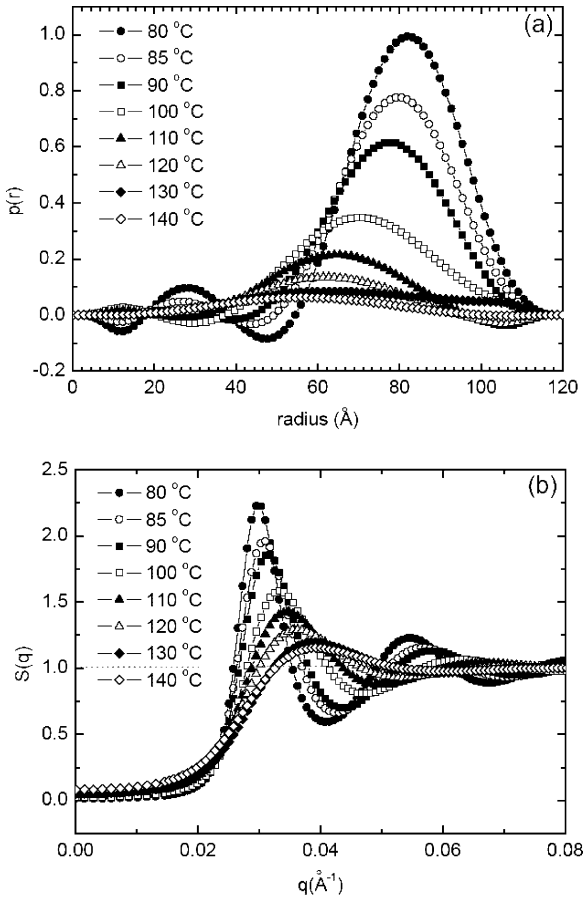

Figure 9. Representative (a) pair distance distribution functions, $p(r)$ and (b) structure factors $S(q)$ obtained from the GIFT at indicated temperatures for a 40% SdI(15−14) in DEP/DBP (75/25 vol %) solution.

Table 6. Summary of the Direct Spherical Model Fits for a 40% SdI(15−14) in DEP/DBP (75/25 vol %)

T, °C	R_c, Å	R_{hs}, Å	$R_{hs} - R_c$, Å	N_{agg}	$\phi_{core,\,sol}$	σ_c	ϕ_{hs}
80	79.3	120.5	41.2	56	0.366	7.7	0.520
85	77.5	117.2	39.7	51	0.384	7.8	0.495
90	74.8	112.0	37.2	45	0.395	7.6	0.473
100	68.5	106.3	37.8	32	0.427	9.4	0.438
110	60.7	100.1	39.4	21	0.473	8.9	0.383
120	60.4	95.0	34.6	18	0.549	11.4	0.367
130	60.5	90.8	30.3	17	0.568	13.9	0.339
140	55.9	88.4	32.5	12	0.609	14.1	0.308

The direct model fitting was carried out with a spherical form factor (eq 9) along with the PY structure factor (eq 11) with the core size polydispersity (eq 10) and the instrumental smearing effects (eq 13) taken into account. One might imagine that the hex phase could disorder into wormlike micelles rather than spheres. Accordingly, we also tried the direct model fitting with an ellipsoidal form factor, considering the ellipticity of micelles, ϵ, as follows:[53]

$$P_{core}(q) = \int_0^{\pi/2} P^2[q, r(R, \epsilon, \alpha)]\sin\alpha d\alpha \qquad (15)$$

$$r(R, \epsilon, \alpha) = R(\sin^2\alpha + \epsilon^2\cos\alpha)^{1/2} \qquad (16)$$

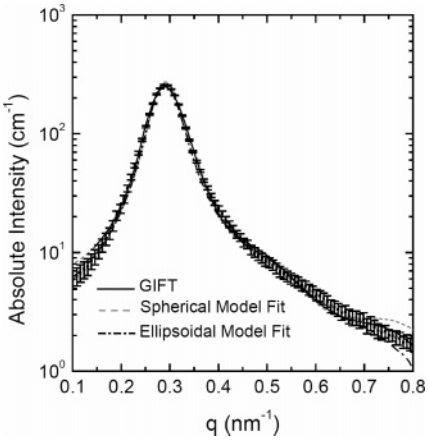

Figure 10. SANS scattering profile for a 40% S*d*I(15−14) in DEP/DBP (75/25 vol %) solution at 80 °C filled with the GIFT and the PY effective hard-sphere model with spherical and ellipsoidal form factors.

However, we were unable to find a better fit than with the spherical form factor. The best fit with the ellipsoidal form factor is obtained with $\epsilon = 1.3$. Figure 10 shows representative fitting results for the SANS profile taken at 80 °C. Both GIFT and direct model fitting yields good agreement with the experimental data. The aggregation number of the micelles is again estimated by allowing the presence of solvent in the micellar core (eq 14), and the calculated values are also summarized in Table 6. With increasing temperature, the aggregation number steadily decreases with the increased solvent swelling of the core. At the cmt, the obtained aggregation number is about 30 and the volume fraction of solvent is as high as 40%, implying denser micellar cores compared with the 25% solution. Upon further heating, the aggregation number decreases close to 10 and more than 50% solvent exists in the micelle core indicating a significant fraction of free chains in solution with increasing temperature. Again, the micelles were found to dissociate into free chains at approximately 20 °C higher than T_{ODT} and the mean-field fits above T_{MF} will be described below.

Crossover from Disordered Micelles to Mean-Field Regime above the cmt. $I(q)$ from a block copolymer solution in the disordered state within the mean-field regime is described by[54]

$$I(q) \sim [S(q)/W(q) - 2\chi_{eff}]^{-1} \tag{17}$$

where $S(q)$ is the sum of all elements and $W(q)$ is the determinant of the matrix:

$$S(q) = S_{AA}(q) + S_{BB}(q) + 2\,S_{AB}(q) = Ng(1) \tag{18}$$

$$W(q) = S_{AA}(q)S_{BB}(q) - S_{AB}{}^2(q) \tag{19}$$

with

$$S_{AA}(q) = Ng(f) \tag{20}$$

$$S_{BB}(q) = Ng(1-f) \tag{21}$$

$$S_{AB}(q) = N/2[g(1) - g(f) - g(1-f)] \tag{22}$$

$$g(f) = (2/x^2)[fx + \exp(-fx) - 1] \tag{23}$$

$$x = q^2R_g{}^2 \tag{24}$$

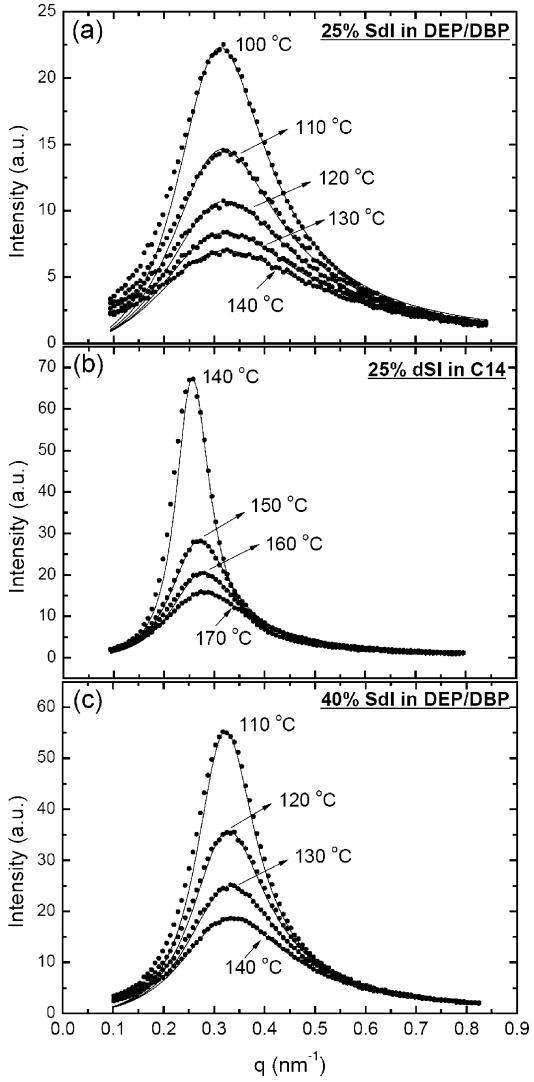

Figure 11. SANS profiles at different temperatures above the cmt for (a) a 25% S*d*I(15−14) in DEP/DBP (75/25 vol %), (b) a 25% *d*SI(16−15) in C14/*d*C14 (90/10 vol %), and (c) a 40% S*d*I(15−14) in DEP/DBP (75/25 vol %). The solid lines show the scattering profiles predicted from the Leibler−Landau mean-field theory in disordered state.

Since $I(q)$ defined by eqs 17−24 is only applied to monodisperse systems, we extended the Leibler−Landau-type mean-field theory[1] for the disordered regime accounting for the effect of polydispersity in the molecular weight and the solvent effect, which have previously been demonstrated to be important in some cases.[55] Accordingly, $g(f)$ is replaced by

$$Ng(f) = 2N_n/x^2\{fx - 1 + [k/(k+fx)]^k\} \tag{25}$$

with

$$N_n = (\rho_{PS}\rho_{PI})^{1/2}(N_{n,PS}/\rho_{PS} + N_{n,PI}/\rho_{PI}) \tag{26}$$

$$N_w/N_n = (k+1)/k \tag{27}$$

where ρ_{PS} and ρ_{PI} are the segmental densities of PS and PI: $\rho_{PS} = 1.01 \times 10^{-2}$ mol/m^3; $\rho_{PI} = 1.34 \times 10^{-2}$ mol/m^3 (for 1,4-addition).[22] In our system, the polydispersity index is found to be 1.04 for both S*d*I(15−14) and *d*SI-(16−15) with $k \approx 25$.

Figure 11 shows the scattering profiles from 25% S*d*I in DEP/DBP, 25% *d*SI in C14/*d*C14, and 40% S*d*I in

Table 7. Summary of the Leibler−Landau Fit Results for 25% S*d*I(15−14) in DEP/DBP (75/25 Vol %), 25% *d*SI(16−15) in C14/*d*C14 (90/10 vol %), and 40% S*d*I(15−14) in DEP/DBP (75/25 vol %)

	R_g, Å		
T, °C	25% S*d*I(15−14) in DEP/DBP	25% *d*SI(16−15) in C14/*d*C14	40% S*d*I(15−14) in DEP/DBP
100	60		
110	58		58
120	58		57
130	58		56
140	58	72	56
150		69	
160		67	
170		67	

DEP/DBP solutions in the disordered state above the cmt as a function of temperature. The solid lines are obtained by the fitting with eqs 17−27, and the results are summarized in Table 7. All the solutions given in Figure 11 show scattering profiles with single peaks. According to the mean-field theory the scattering vector at the intensity maximum I_{max}, q_{max}, is independent of temperature and the I_{max} decreases as temperature T is increased. The q_{max} is also related to the correlation holes reflecting the dominant mode of concentration fluctuations on the scale of R_g. It is particularly interesting to note that three solutions in Figure 11 show the temperature independence of q_{max} at high temperature, which is in agreement with the Leibler−Landau theory, and as the temperature is lowered there exists an onset temperature at which the q_{max} deviates from the q_{max} at the high temperature (also see Table 7). The small shift in q_{max} reflects the incipient point of the nonmean-field effect.[3] Accordingly, the T_{MF} can be accurately determined by this criterion and the T_{MF} values thus determined are between 100 and 110 °C for a 25% S*d*I in DEP/DBP, between 150 and 160 °C for a 25% *d*SI in C14/*d*C14, and between 120 and 130 °C for a 40% solution of S*d*I in DEP/DBP, which are in excellent agreement with the values obtained by the I_{max}^{-1} vs T^{-1} plots shown in Figures 2, 6, and 8. The comparison between the experimental data and the theoretical predictions also shows some deviations at low q ($<q_{max}$), and this discrepancy at low q tends to increase with increasing temperature. We tentatively attribute this to an increased contribution of concentration fluctuations between solvent and copolymer chains.[22]

On the basis of these experimental results, a schematic illustrating the regions of the micelles in long-range order, the disordered micelles, and the dominant free chains along with associated transitions is given in Figure 12. For S*d*I(15−14) in DEP/DBP, the solution with polymer volume fraction $\phi = 0.25$ adopts the bcc structure while for $\phi = 0.40$, the hex phase is observed. The long-range order for both bcc and hex phases is maintained up to the T_{ODT}, at which the long-range lattice order is lost. At approximately 20−30 °C higher than T_{ODT}, the disordered micelles were found to dissociate into free chains, which is defined as the cmt in present study. As a result, upon heating from a low-temperature ordered state, the balance between the chains in micelles and the free chains is shifted toward the free chains, eventually disrupting all the micelles at around T_{MF}. The observed phase sequence is similar to that in bcc-forming block copolymer melts:[26,30−33] one thermodynamic phase transition, the ODT, and one phenomenological transition, the cmt, which lies within the disordered phase.

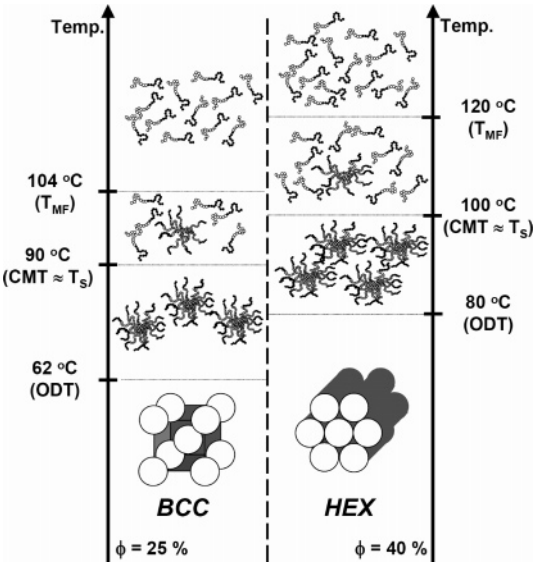

Figure 12. Phase behavior for 25% S*d*I(15−14) in DEP/DBP (75/25 vol %) and 40% S*d*I(15−14) in DEP/DBP (75/25 vol %). Bcc and HEX denote the body-centered cubic and the hexagonal cylinder, respectively, and ODT, cmt, T_S, and T_{MF} for the two solutions are shown. A schematic illustrating the regions of the micelles in long-range order, the disordered micelles along with associated transitions is also given.

Conclusions

1. We have examined the solution behavior just above T_{ODT} by SANS with symmetric PS-*d*PI and *d*PS−PI diblock copolymers in selective solvents. The model-independent GIFT of the experimental data and the direct model fitting with appropriate form factors and structure factors were employed to analyze the SANS data to make a close investigation of the solution behavior in the disordered micelle regime.

2. The micelles were found to break up into free chains at the cmt, which is experimentally determined by an abrupt decrease in the size, aggregation number, and volume fraction of micelles and is close to T_S. Notably, regardless of different ordered microstructures prior to the disordered state, i.e., bcc and hex, the cmt is approximately 20−30 °C higher than T_{ODT}.

3. It is interesting to note that for solutions undergoing the bcc-to-disorder transition, a clear crossover behavior of the domain spacing (D) upon heating across the T_{MF} was observed. However, the slope of D vs T^{-1} does not change around T_{MF} for the hex-to-disorder transition. In addition, for the hex-to-disorder transition, the cmt is harder to locate compared with bcc-to-disorder transition. Interestingly, even in this case the disordered micelles were approximately spherical.

4. Two transitions, one between ordered phase and disordered micelles (ODT) and the other between disordered micelles and disorder (cmt) were identified and consequently, three clear regimes were discussed: *ordered*−ODT−*disordered micelles*−cmt−*mean field regime*.

Acknowledgment. This work was supported primarily by the MRSEC program of the National Science Foundation under Award DMR-0212302. We are grateful to the financial support from the National Research Laboratory Fund (Grant M1-0104-00-0191) from the Ministry of Science and Technology of Korea and the Brain Korea 21 Program endorsed by the Ministry of Education of Korea. Further support for this research

was provided by the National Institute of Standards and Technology, U.S. Department of Commerce, through the neutron research facilities.

References and Notes

(1) Leibler, L. *Macromolecules* **1980**, *13*, 1602.
(2) Helfand, E.; Wasserman, Z. R. *Developments in Block Copolymers*; Goodman, I., Ed.; Applied Science: New York, 1985; Chapter 4.
(3) Fredrickson, G. H.; Helfand, E. *J. Chem. Phys.* **1987**, *87*, 697.
(4) Brown, R. A.; Masters, A. J.; Price, C.; Yuan, X. F. In *Comprehensive Polymer Science*; Booth, C.; Price, C., Eds.; Pergamon Press: Oxford, U.K., 1989; Vol. 2.
(5) Tuzar, Z.; Kratochvil, P. In *Surface and Colloid Science*; Matijevic, E., Ed.; Plenum Press: New York, 1993; Vol. 15.
(6) Mortensen, K.; Pedersen, J. S. *Macromolecules* **1993**, *26*, 805.
(7) Mayes, A. M.; Barker, J. G.; Russell, T. P. *J. Chem. Phys.* **1994**, *101*, 5213.
(8) Lodge, T. P.; Xu, X.; Ryu, C. Y.; Hamley, I. W.; Fairclough, J. P. A.; Ryan, A. J.; Pedersen, J. S. *Macromolecules* **1996**, *29*, 5955.
(9) Adams, J. L.; Quiram, D. J.; Graessley, W. W.; Register, R. A.; Marchand, G. R. *Macromolecules* **1996**, *29*, 2929.
(10) Schwab, M.; Stühn, B. *Phys. Rev. Lett.* **1996**, *76*, 924.
(11) Maurer, W. W.; Bates, F. S.; Lodge, T. P.; Almdal, K.; Mortensen, K.; Fredrickson, G. H. *J. Chem. Phys.* **1998**, *108*, 2989.
(12) Bates, F. S.; Rosedale, J. H.; Fredrickson, G. H.; Glinka, C. J. *Phys. Rev. Lett.* **1988**, *61*, 2229.
(13) Bates, F. S.; Rosedale, J. H.; Fredrickson, G. H. *J. Chem. Phys.* **1990**, *92*, 6255.
(14) Rosedale, J. H.; Bates, F. S. *Macromolecules* **1990**, *23*, 2329.
(15) Almdal, K.; Bates, F. S.; Mortensen, K. *J. Chem. Phys.* **1992**, *96*, 9122.
(16) Rosedale, J. H.; Bates, F. S.; Almdal, K.; Mortensen, K.; Wignall, G. D. *Macromolecules* **1995**, *28*, 1429.
(17) Frielinghaus, H.; Schwahn, D.; Mortensen, K.; Almdal, K.; Springer, T. *Macromolecules* **1996**, *29*, 3263.
(18) Holmqvist, P.; Pispas, S.; Hadjichristidis, N.; Fytas, G.; Sigel, R. *Macromolecules* **2003**, *36*, 830.
(19) Guenza, M.; Schweizer, K. S. *J. Chem. Phys.* **1997**, *106*, 7391.
(20) Guenza, M.; Schweizer, K. S. *Macromolecules* **1997**, *30*, 4205.
(21) Almdal, K.; Mortensen, K.; Ryan, A. J.; Bates, F. S. *Macromolecules* **1996**, *29*, 5940.
(22) Mori, K.; Okawara, A.; Hashimoto, T. *J. Chem. Phys.* **1996**, *104*, 7765.
(23) Adams, J. L.; Graessley, W. W.; Register, R. A. *Macromolecules* **1994**, *27*, 6026.
(24) Zhao, J.; Majumdar, B.; Schulz, M. F.; Bates, F. S.; Almdal, K.; Mortensen, K.; Hajduk, D. A.; Gruner, S. M. *Macromolecules* **1996**, *29*, 1204.
(25) Lee, S.-H.; Char, K.; Kim, G. *Macromolecules* **2000**, *33*, 7072.
(26) Dormidontova, E. E.; Lodge, T. P. *Macromolecules* **2001**, *34*, 9143.
(27) Sota, N.; Sakamoto, N.; Saijo, K.; Hashimoto, T. *Macromolecules* **2003**, *36*, 4534.
(28) Sakamoto, N.; Hashimoto, T.; Han, C. D.; Kim, D.; Vaidya, N. Y. *Macromolecules* **1997**, *30*, 1621.
(29) Sakamoto, N.; Hashimoto, T.; Han, C. D.; Kim, D.; Vaidya, N. Y. *Macromolecules* **1997**, *30*, 5321.
(30) Han, C. D.; Vaidya, N. Y.; Kim, D.; Shin, G.; Yamaguchi, D.; Hashimoto, T. *Macromolecules* **2000**, *33*, 3767.
(31) Wang, X.; Dormidontova, E. E.; Lodge, T. P. *Macromolecules* **2002**, *35*, 9687.
(32) Bodycomb, J.; Yamaguchi, D.; Hashimoto, T. *Macromolecules* **2000**, *33*, 5187.
(33) Wang, J. F.; Wang, Z.-G.; Yang, Y. L. *Macromolecules*, in press.
(34) Semenov, A. N. *Macromolecules* **1989**, *22*, 2849.
(35) Matsen, M. W.; Bates, F. S. *Macromolecules* **1996**, *29*, 1091.
(36) Matsen, M. W.; Bates, F. S. *J. Chem. Phys.* **1997**, *106*, 2436.
(37) Shibayama, M.; Hashimoto, T.; Kawai, H. *Macromolecules* **1983**, *16*, 16.
(38) Hashimoto, T.; Shibayama, M.; Kawai, H. *Macromolecules* **1983**, *16*, 361.
(39) Hamley, I. W.; Fairclough, J. P. A.; Ryan, A. J.; Ryu, C. Y.; Lodge, T. P.; Gleeson, A. J.; Pedersen, J. S. *Macromolecules* **1998**, *31*, 1188.
(40) Hanley, K. J.; Lodge, T. P.; Huang, C.-I. *Macromolecules* **2000**, *33*, 5918.
(41) Lodge, T. P.; Hanley, K. J.; Pudil, B. *Macromolecules* **2002**, *35*, 4707.
(42) Bang, J.; Viswanathan, K.; Lodge, T. P.; Park, M. J.; Char, K. *J. Chem. Phys.* **2004**, *121*, 11489.
(43) Jackson, C.; Nillson, L.; Wyatt, P. J. *J. Appl. Polym. Sci.* **1991**, *42*, 217.
(44) Huglin, M. B. *Light Scattering from Polymer Solution*; Academic: New York, 1972.
(45) Park, M. J.; Bang, J.; Harada, T.; Lodge, T. P.; Char, K. *Macromolecules* **2004**, *37*, 9064.
(46) Brunner-Popela, J.; Glatter, O. *J. Appl. Crystallogr.* **1997**, *30*, 431.
(47) Hansen, J. P.; McDonald, I. R. In *The Theory of Simple Liquids*; Academic: London, 1990.
(48) Brunner-Popela, J.; Mittelbach, R.; Strey, R.; Schubert, K.-V.; Kaler, E. W.; Glatter, O. *J. Chem. Phys.* **1999**, *21*, 10623.
(49) Weyerich, B.; Brunner-Popela, J.; Glatter, O. *J. Appl. Crystallogr.* **1999**, *32*, 197.
(50) Pedersen, J. S.; Gerstenberg, M. C. *Macromolecules* **1996**, *29*, 1363.
(51) Pedersen, J. S. *J. Chem. Phys.* **2001**, *114*, 2839.
(52) Pedersen, J. S.; Posselt, D.; Mortensen, K. *J. Appl. Crystallogr.* **1990**, *23*, 321.
(53) Feigin, L. A.; Svergun, D. I. In *Structure Analysis by Small-Angle X-ray and Neutron Scattering*; Plenum Press: New York, 1987.
(54) Benmouna, M.; Wu, W.; Mozer, B.; Bauer, B.; Lapp, A. *Macromolecules* **1985**, *18*, 986.
(55) Sakurai, S.; Mori, K.; Okawara, A.; Kimishima, K.; Hashimoto, T. *Macromolecules* **1992**, *25*, 2679.

MA0477044